THE JOURNAL OF PHYSICAL CHEMISTRY C

ARTICLE

pubs.acs.org/JPCC

Tuning the Conduction Mechanism in Niobium-Doped Titania Nanoparticle Networks

Hynek Němec,* Zoltán Mics, Martin Kempa, and Petr Kužel

Institute of Physics, Academy of Sciences of the Czech Republic, Na Slovance 2, 18221 Prague 8, Czech Republic

Oliver Hayden

Corporate Technology, Siemens AG, CT T DE HW3, Guenther-Scharowsky-Strasse 1, 91050 Erlangen, Germany

Yujing Liu, Thomas Bein, and Dina Fattakhova-Rohlfing

Department of Chemistry and Biochemistry, University of Munich, Butenandtstrasse 5-13, 81377 Munich, Germany

ABSTRACT: Networks of niobium-doped TiO_2 anatase nanoparticles with variable doping concentrations were investigated by time-domain terahertz spectroscopy and microwave impedance spectroscopy. A detailed description of their electromagnetic response is proposed; the model takes into account the depolarization fields of inhomogeneous samples and allows us to understand the conductive and dielectric response of individual nanoparticles. We find that electron hopping is the dominating contribution to the conductivity at terahertz frequencies and that the dielectric losses of TiO_2 nanoparticles are enhanced in comparison with bulk anatase. The conductive properties of nanoparticles can be tuned via synthesis conditions and thermal posttreatment. In particular, annealing at elevated temperatures improves the nanoparticle crystallinity, reduces the density of structural defects, and enhances the conductive percolation of the network. The developed model of the conduction processes can be helpful for interpretation of charge transport in other semiconducting nanoscale materials.

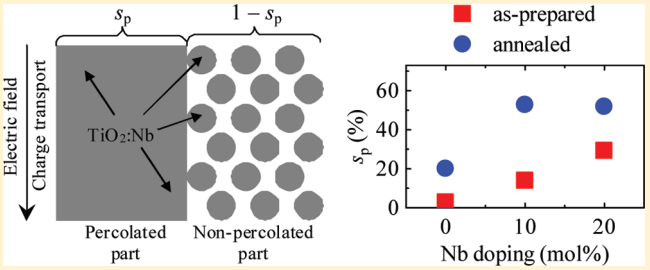

1. INTRODUCTION

Nanoscaling and nanopatterning introduce additional functional properties to existing materials, which opens a way to the conception of novel devices and techniques. For example, fabrication of transparent conducting oxides in the form of nanoparticles can significantly enrich the scope of the available materials in addition to dense films, enabling manufacturing of conducting composites, nanostructured transparent electrodes, or low-temperature printing of patterned electrodes. However, the decrease of grain dimensions to the nanoscale increases the role of the surface, which dramatically alters the dielectric properties and electron transport in the nanoparticle-based materials. The measured macroscopic conductivity in a sample composed of assembled nanosized particles is influenced (besides the intrinsic bulk properties of the material) by several factors such as electron confinement effects, energy of surface states, difference in surface and core composition of nanoparticles, electron scattering on surface defects and on grain boundaries, and connectivity of nanoparticles in the sample, just to name a few. The ability to resolve and characterize the individual factors controlling the total macroscopic conductivity is of extreme importance for the optimization of charge carrier transport properties in nanoscaled materials.

Many of these factors can be assessed from the electromagnetic response measured in a broad frequency range. A very pertinent spectral domain for the investigation of nanoscaled materials is the terahertz (THz) range. First of all, different conductivity mechanisms lead to qualitatively different conductivity spectra in the terahertz region, and it is straightforward to distinguish between the response of delocalized electrons (described, for example, by the Drude formula) and electrons localized in potential wells.[1,2] The electron confinement strongly affects the conductivity spectra if the particle size is comparable to or smaller than the electron diffusion length l_D on the time scale of one period of the probing radiation [$l_D \approx (D/f)^{1/2}$, where D is the diffusion coefficient and f is the probing frequency]. Terahertz frequencies are thus optimal for the investigation of electron transport within and among nanometer-sized particles of common semiconductors.[3] Finally, the measured conductivity spectra reflect the distribution of depolarization fields, which are inherently related to the morphology of the nanomaterial.[4,5]

Received: January 26, 2011
Revised: February 15, 2011
Published: March 04, 2011

In this sense, the terahertz spectral region contains rich information about nanoscale systems, covering conductivity mechanisms, carrier confinement, and material morphology.[6] However, full quantitative interpretation of the conductivity spectra requires the development of a microscopic theoretical framework able to describe all the above-mentioned phenomena and to extract their respective contributions from the measured spectra. Despite the great potential of terahertz spectroscopy in the field of nanoscaled materials, such an approach has been seldom applied up to now (see ref4 and references therein).

Niobium-doped titanium dioxide (NTO) is a novel class of transparent conductors, which is considered as a cheap and chemically stable alternative to indium tin oxide.[7] Recently, we described a low-temperature synthesis approach for the fabrication of monosized dispersible crystalline NTO particles of just a few nanometers in size with different Nb contents, which can be assembled into mesoporous films with periodic porous architectures.[8] We observed that the Nb doping of the titania lattice leads to the introduction of donor levels into TiO_2, detectable as the reduced states of the Ti and Nb, and to a drastic increase in the electrical direct current (dc) conductivity. Its dependence on the Nb doping level in the nanoparticles is, however, different from that in bulk materials fabricated by physical methods such as pulsed laser deposition or high-temperature solid-state synthesis, and it is strongly influenced by the synthesis temperature and heat treatment conditions. In order to understand the conductivity mechanisms in this system, it is important to identify the different contributions to the conductivity by measurements over a broad range of frequencies. The resulting picture of the conduction processes can be helpful for interpretation of charge transport in other semiconducting nanoscale materials.

In this paper, we employ time-domain terahertz spectroscopy and microwave impedance spectroscopy to measure the conductivity and permittivity spectra in the terahertz and gigahertz spectral regions for a set of pellets of Nb-doped anatase nanoparticle networks with variable doping concentrations. We develop a detailed physical framework for the interpretation of the conductivity spectra where we establish the relationship between depolarization fields and sample morphology, characterize the electron confinement, and identify the relevant conductivity mechanisms.

2. EXPERIMENTAL RESULTS

TiO_2 nanoparticles were prepared by a nonaqueous synthesis at 60−150 °C via solvothermal procedures with *tert*-butanol as a reaction medium and three Nb doping levels (0, 10, and 20 mol %): for details see ref 8. Pellets were formed by pressing the nanoparticles under a pressure of 10 MPa in a sample holder 13 mm in diameter; their thickness ranged from 0.55 to 1.28 mm. Pellets were studied as prepared and annealed at 600 °C under nitrogen atmosphere to prevent oxidation and water vapor adsorption.

The elaboration procedure enables preparation of nonagglomerated nanoparticles, whose size and crystallinity can be controlled by the reaction temperature and time. At 60 °C, completely amorphous particles are obtained. An increase of the reaction temperature to 100 °C leads to the formation of ∼4 nm crystalline nanoparticles with a phase structurally related to anatase, which can incorporate more than 20 mol % of Nb ions without significant distortion of the anatase lattice or phase separation. The introduction of Nb in the anatase lattice increases the dc conductivity by several orders of magnitude.[8] The dc conductivity of the pellets pressed from the particles prepared at 100 °C is 1×10^{-6} S·cm^{-1} for undoped and 2×10^{-5} S·cm^{-1} for the 20% doped nanoparticles. Heating of the as-produced NTO nanoparticles at 600 °C under nitrogen atmosphere further improves the dc electrical conductivity, which increases up to 0.25 S·cm^{-1} for the 20% Nb sample. The onset of dc conductivity in the Nb-doped particles is supported by an observation of reduced states of both titanium and niobium, Ti^{3+} and Nb^{4+} or lower, by X-ray photoelectron spectroscopy (XPS). The presence of these states in both as-prepared and heated particles enabled us to suggest that most of the extra electrons generated by Nb doping are released into the conduction band of TiO_2, leading to the formation of Ti^{3+} and resulting in electrical conductivity.[8]

To evaluate the role of Nb doping in the conductivity at terahertz frequencies, we selected a set of nanoparticles synthesized under the same reaction conditions, namely at 100 °C, and with the Nb content varying from 0% to 20% (denoted further as NTO_*X*%@100 °C). The particles prepared in this way are crystalline, of about 4 nm diameter. Additionally, in order to investigate the role of crystallization conditions in the conductivity of samples prepared from different types of particles, we prepared the NTO particles with a single doping level of 20 mol % but at different synthesis temperatures, 60 and 150 °C, (denoted further as NTO_20%@60 °C and NTO_20%@150 °C), which leads to the formation of amorphous and completely crystalline particles, respectively. The particles were pressed into pellets and studied as prepared and after heating in nitrogen at 600 °C.

The permittivity and conductivity at terahertz frequencies were measured by time-domain terahertz transmission spectroscopy.[9] The useful bandwidth in our custom-made setup, based on a femtosecond laser oscillator, spans from 0.1 to 3 THz.[10] The permittivity and conductivity spectra were retrieved from the directly measured complex transmittance spectra of terahertz radiation (i.e., in a noncontact fashion). These results are free of systematic errors related to electrodes and they are also very accurate.[9−11] The method provides the dielectric permittivity averaged over the entire thickness of the sample.

The impedance at microwave frequencies (20 MHz−10 GHz) was measured by an open-end coaxial technique (Agilent 85070E dielectric probe) with an Agilent E8364B network analyzer. The drawback of this technique is the difficult control of the quality of the contact between probe and sample. Our samples are very rigid and their surface is rough. Under these conditions, it is rather difficult to obtain a good electrical contact. In fact, most of the measured microwave permittivities are lower than the terahertz permittivity, which indicates that an air gap or dead layer was formed between the sample and the end of the probe. As a result, measurements of the microwave permittivity provide a good indication of the trends in the permittivity spectra, but the data are not accurate enough to be used for a common fitting with the terahertz data.

The permittivity spectra measured by microwave and terahertz spectroscopy are summarized in Figures 1 and 2. All the samples exhibit qualitatively similar behavior. At microwave frequencies, both the real and imaginary parts of the permittivity decrease with increasing frequency. This behavior is characteristic for a broadband dielectric relaxation. In principle, such a relaxation could originate from lattice dynamics. However, the lattice response of anatase is dominated by phonon modes and no relaxation is observed in bulk crystals.[12] We thus attribute the

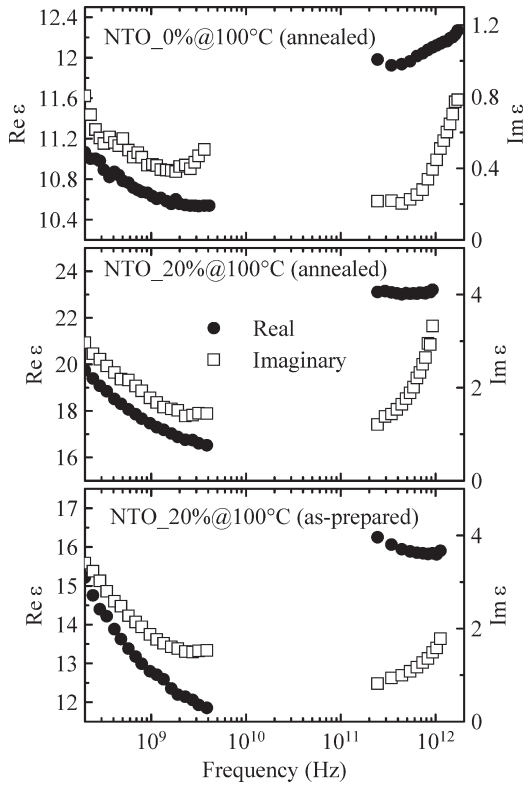

Figure 1. Measured (●) real and (□) imaginary parts of the permittivity of selected samples. Gigahertz spectra were measured by the microwave impedance analyzer, whereas terahertz spectra were measured by time-domain terahertz spectroscopy.

observed broadband response to an electron hopping with a wide distribution of hopping times.[13]

For as-prepared particles with different Nb doping levels, the real part decreases continuously up to 0.4−1 THz, whereas at higher frequencies it starts to increase. Similar but less-pronounced trends are observed in the spectra of annealed samples (note that the accessible spectral range is narrower due to their stronger absorption). The imaginary part of the permittivity increases with frequency in the terahertz region in all samples. The decreasing real part is the tail of the broadband response due to the hopping conduction. The slight parabolic increase in the real part, accompanied by the almost linearly increasing imaginary part, is naturally explained as the onset of the phonon contribution to this part of the spectrum.[12]

3. MODEL OF THE DIELECTRIC FUNCTION

On the basis of the above considerations, we developed a model of the dielectric permittivity that allows us to get a more detailed qualitative and quantitative understanding of the observed response in all samples. This model takes into account factors that may influence the macroscopic permittivity (conductivity) of the particles pressed into pellets, namely: (i) permittivity and conductivity of individual nanoparticles and (ii) the inhomogeneous nature of the pellets.

i. Permittivity of Individual Nanoparticles. The response of the doped titania consists of lattice and electron contributions. As we have pointed out above, the former is related to a polar phonon mode, whereas electron hopping dominates the latter contribution.

Anatase is a uniaxial crystal with static relative permittivities of $\varepsilon_{c,0} = 45.1$ and $\varepsilon_{a,0} = 22.7$ for the electric field polarized along and perpendicularly to the optical axis, respectively, and with different phonon modes in the polarized infrared spectra for these two polarizations.[12] For simplicity, we approximate the permittivity of anatase as the average of the diagonal tensor elements: $\varepsilon_{\text{anatase}} = (2\varepsilon_a/3) + (\varepsilon_c/3)$. The static average relative permittivity of anatase is then $\varepsilon_{\text{anatase},0} = 37.6$.

For the hopping conductivity spectra, we employ Dyre's random free-energy model:[14]

$$\sigma_{\text{hopping}}(f) = 2\pi i f \sigma_\infty \left[1 - \frac{\ln\dfrac{\tau_{\min}}{\tau_{\max}}}{\ln\dfrac{1-2\pi i f\tau_{\min}}{1-2\pi i f\tau_{\max}}}\right] \frac{\ln\dfrac{\tau_{\max}}{\tau_{\min}}}{\dfrac{1}{\tau_{\min}} - \dfrac{1}{\tau_{\max}}} \quad (1)$$

which does not exhibit the conductivity divergence encountered, for example, in a power-law ($\sigma \propto \omega^s$) model. The spectrum of the hopping conductivity (eq 1) is sketched in Figure 3. At frequencies well above the electron hopping rate $1/\tau_{\min}$, the conductivity approaches a constant value of σ_∞, which we will call a "saturated conductivity" in the subsequent discussion. The time $\tau_{\max}$ represents the longest waiting time found in the system and it delimits the range of dispersion at low frequencies—the conductivity is constant and low below $1/\tau_{\max}$. The dc conductivity $[\sigma_{\text{hopping}}(0)]$ decreases with increasing $\tau_{\max}$.

The total permittivity of individual conducting nanoparticles reflecting both the lattice and the electron contribution then reads $\varepsilon = \varepsilon_{\text{anatase}} + i\sigma_{\text{hopping}}/(2\pi f\varepsilon_0)$.

ii. Permittivity of the Pellets. A substantial complication in the analysis of the measured permittivity is imposed by the inhomogeneous nature of the pellets, which gives rise to depolarization fields.[5] Since the nanoparticles are much smaller than the wavelength of the incident radiation, we use an effective medium approximation that yields a relationship between the permittivity of nanoparticles and the effective (measured) permittivity of the samples. The effective medium approximation should account for the broad range of the observed permittivity values: these span from ∼7.0 for the as-prepared NTO_0%@100 °C sample to ∼27.8 for the annealed NTO_20%@60 °C sample (Figure 2). Different dilutions of anatase nanoparticles cannot be responsible for this large difference, since the mass densities of all pellets are roughly comparable to each other. The observed differences in the permittivities thus necessarily originate from different degrees of dielectric percolation of nanoparticles. For example, the permittivity value of the annealed sample NTO_20%@60 °C is quite close to the average permittivity of the anatase (∼37.6), which shows that a significant fraction of the titania is percolated in this sample. Conversely, the low permittivity observed in the undoped crystalline sample NTO_0%@100 °C indicates that the titania is not percolated: individual titania nanoparticles are isolated from each other by a low-permittivity organic shell or by a low-permittivity dead layer. In order to account for both these extreme cases, we express the effective permittivity ε_{eff} as a sum of these two contributions, which is analogous to a parallel connection of two capacitors (Figure 4):[15]

$$\varepsilon_{\text{eff}} = s_p\varepsilon_{\text{percolated}} + (1 - s_p)\varepsilon_{\text{nonpercolated}} \quad (2)$$

Here $\varepsilon_{\text{percolated}} = \varepsilon$ is the permittivity of the percolated part, which is equal to the permittivity of the anatase nanoparticles ε, and s_p is the volume fraction of the percolated part. The

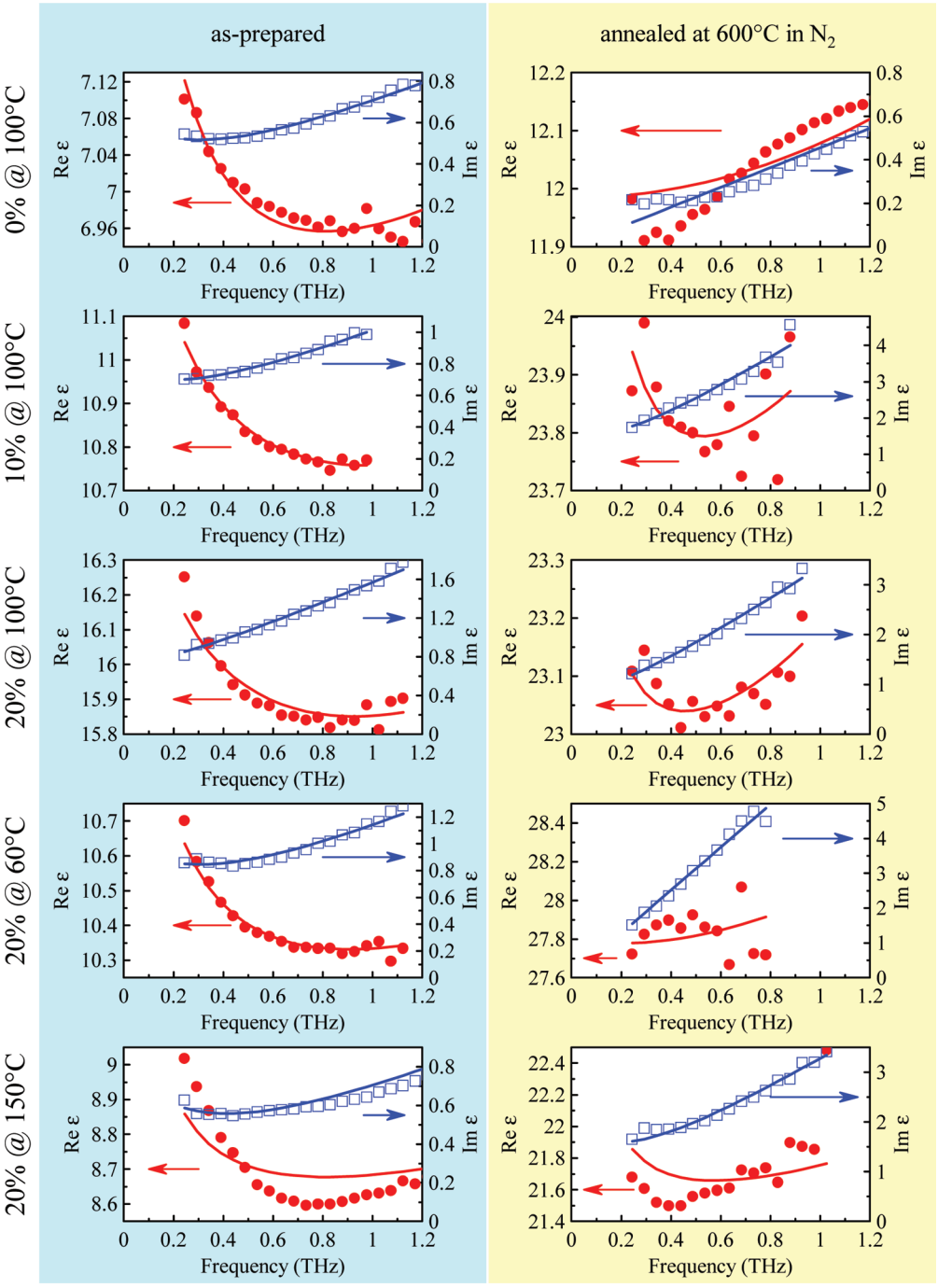

Figure 2. Complex permittivity in the terahertz spectral range. (Symbols) Measurement by time-domain terahertz spectroscopy; (—) fit by eq 2. Red circles correspond to the real part and blue squares represent the imaginary part of the permittivity.

permittivity of the nonpercolated part is calculated within the Maxwell−Garnett model, which assumes no dielectric connectivity between the nanoparticles:

$$\varepsilon_{\text{nonpercolated}} = \frac{\varepsilon(1+2s_n)+2(1-s_n)}{\varepsilon(1-s_n)+(s_n+2)} \qquad (3)$$

The nonpercolated titania nanoparticles are assumed to occupy a volume fraction $s_n = 0.65$ (tightly packed spheres), whereas the rest of the space is occupied by a material with permittivity close to 1 (air pores, residual organic parts). It should be noted that the permittivity ε is frequency-dependent; eq 3 then implies that its shape generally differs from the spectrum of the effective permittivity ε_{eff}.[4]

4. DISCUSSION

For fitting of the experimental spectra in the terahertz range, the model described by eq 2 was used. The charge carrier hopping rate τ_{min} in eq 1 was set to 20 fs, which corresponds to the phonon frequency,[13] whereas τ_{max} was kept at 100 ns, which is well below the available spectral window (this parameter

dx.doi.org/10.1021/jp200822y |J. Phys. Chem. C 2011, 115, 6968–6974

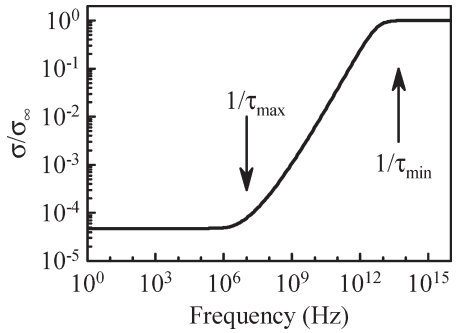

Figure 3. Sketch of the real part of hopping conductivity defined by eq 1 (τ_{min} = 20 fs, τ_{max} = 100 ns). Note that both scales are logarithmic.

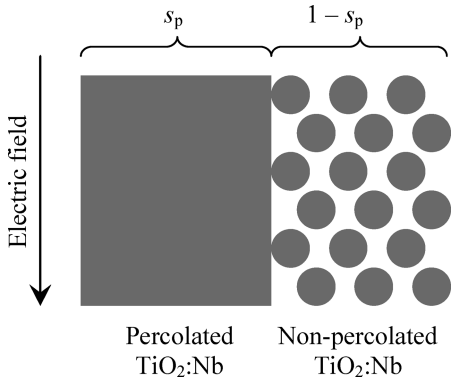

Figure 4. Scheme of the structure proposed to account for the depolarization fields.

has no influence on terahertz spectra). The model described by eq 2 then contains only two adjustable parameters: s_p and σ_∞. However, this model did not yield fully satisfactory results and it turned out to be necessary to enhance by a multiplication factor the anatase dielectric losses related to the phonon mode (Im $\varepsilon_{anatase}$) in order to obtain good fits; we shall refer to this factor as the loss enhancement factor. This enhancement can be understood in terms of extrinsic dielectric losses.[16]

The best fits of the terahertz permittivities by eq 2 are shown in Figure 2. The quality of the fits is very good for most of the nonannealed samples; moreover, extrapolation of the effective permittivity (eq 2) to the microwave region yields a spectrum qualitatively agreeing with that measured by the open-end coaxial probe. The fit of the terahertz data is worse for the NTO_20% @150 °C sample, which is the only nonannealed sample composed of fully crystalline nanoparticles, and for some of the doped samples after annealing. It is then possible that, besides the hopping process, the bandlike transport of electrons starts to significantly contribute to the terahertz conductivity in some of these samples (see discussion below).

The fitting parameters are summarized in Figure 5. The most pronounced trend is the increase of the percolated titania fraction s_p upon annealing. This is related to the sintering and maybe also to a further crystallization and crystal growth of titania nanoparticles. All the Nb-doped annealed samples exhibit a comparable level of the percolated fraction s_p. A significantly lower s_p is observed in the annealed undoped sample. This indicates that Nb doping has a positive effect on nanoparticle sintering. Note that the real morphology of the samples may differ to a certain extent from that sketched in Figure 4. As a result, trends in the

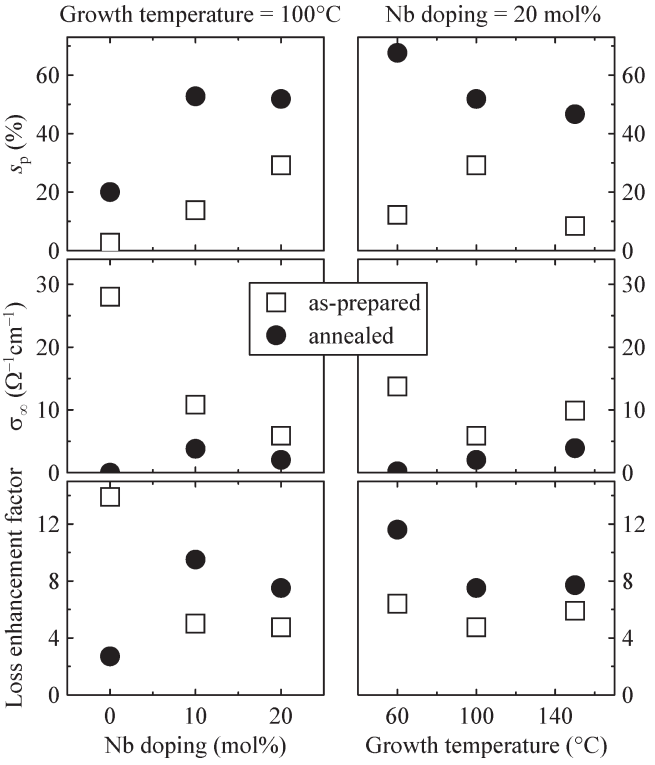

Figure 5. Results of fits of the terahertz permittivity for the pellets pressed from nanoparticles with varying doping levels synthesized at 100 °C (left column), and nanoparticles with 20% doping level synthesized at several temperatures (right column). (□) As-prepared samples, (●) annealed samples.

percolated volume fraction s_p provide reliable information, but its absolute values as well as the absolute value of the total titania fraction, $s_p + s_n(1 - s_p)$, should be taken with care.

The highest value of the saturated conductivity σ_∞ is observed for the as-prepared undoped sample NTO_0%@100 °C, which, surprisingly, exhibits the lowest dc conductivity. This apparent contradiction can be explained in terms of eq 1: this sample must contain a large density of localized states, between which the electron hopping occurs with very long hopping times (high τ_{max}). Such assumptions are well justifiable in the as-prepared nanoparticles, which probably contain a high density of defects: in this case the dc conductivity can be very low. Thermal annealing then removes defects, which in turn may suppress the hopping conductivity. This is observed with the annealed undoped sample NTO_0%@100 °C, where the hopping conductivity is almost zero (Figure 5).

From the data plotted in Figure 5 we see that the saturated hopping conductivity σ_∞ of all doped samples is lower than that of the as-prepared undoped pellet. The saturated hopping conductivity σ_∞ then decreases upon annealing, but it does not vanish. As in the case of the undoped samples, this indicates that a part of the hopping conductivity is related to the existence of defect states that disappear upon thermal annealing. The remaining portion is then induced by the Nb doping. The dc conductivity in the annealed samples is still much lower than the Nb doping-induced hopping conductivity and it is strongly dependent on the doping density. This dependence can be explained through the variation of τ_{max} in eq 1. With increasing doping density, the hopping distance decreases, the

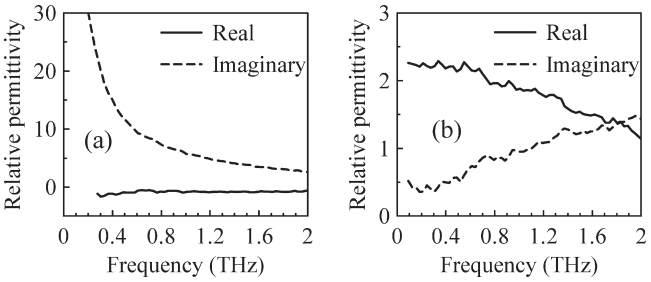

Figure 6. Calculated contribution of conduction-band electrons to the relative permittivity. Parameters: nanoparticle diameter 4.5 nm, electron effective mass $6m_e$, carrier density 3×10^{18} cm^{-3}. (a) Nanoparticle boundaries randomly scatter the carriers. (b) Nanoparticle boundaries reflect the carriers; that is, the carriers are localized within the nanoparticle.

longest hopping time thus shortens, and the dc conductivity is enhanced.

For completeness, we also estimated the possible contribution of *delocalized* conduction band electrons. The conduction band electrons can interact with the nanoparticle surface, which decreases their mobility. The impact of the interaction on the conductivity spectra was studied in detail in ref 3, and we used the same model here in our calculations. The electrons exhibit a Brownian motion within nanoparticles given by isotropic scattering events in the bulk, and in addition, they can interact with the nanoparticle boundaries. In Figure 6 we illustrate the conductivity spectra calculated for two extreme cases: (a) electrons are scattered by the nanoparticle boundary in a random direction, and (b) electrons cannot penetrate through the nanoparticle surface, that is, they are confined within the nanoparticle. These spectra essentially differ from the measured ones (Figure 2), which leads us to the conclusion that band conduction is not dominant at terahertz frequencies. More specifically, the density of delocalized electrons must be significantly lower than 3×10^{18} cm^{-3} used in Figure 6. However, Hall effect measurements show that the electron density is much higher; for example, in the annealed samples with 20 mol % Nb doping, it was $\sim 10^{20}$ cm^{-3}.[8] This means that the vast majority of carriers contribute to the hopping conductivity, which is thus the dominating charge transport mechanism at terahertz frequencies.

Note that from our data it is not possible to distinguish between the bandlike and hopping contributions to the dc conductivity: the longest hopping time τ_{max} (which determines the dc hopping conductivity) cannot be determined from our terahertz measurements, and in our simulations we determined merely the upper limit of the density of delocalized electrons.

The phonon-mode-related dielectric losses are most enhanced in the undoped nonannealed sample (Figure 5); this is consistent with the hypothesis of a high density of defects in the sample. On the other hand, the loss enhancement factor drops to ~3 upon annealing, which is in agreement with the improved crystallinity of annealed anatase grains. The loss enhancement factor for the doped samples is then ~5 before annealing and ~9 after annealing. This suggests that Nb doping leads to a lattice deformation both in as-prepared and in annealed samples and thus to the enhanced dielectric losses. These results show that dielectric losses in semiconductor nanoparticles are enhanced compared to the bulk material. It is not clear whether this is a size effect or an effect due to residual defects present even in the annealed samples.

The obtained results suggest that the doping with Nb in nanosized particles introduces a large amount of reduced states that are observed by XPS, but electrons in these states are rather localized and their dc mobility (not the terahertz one) is rather low. The electron transport in the doped samples is then determined to a significant extent by the hopping between the reduced states. This may explain the fact that the dc conductivity increases significantly with the increasing Nb content and thus with increasing density of the introduced reduced states (which also implies reduction of distances between these states). The increase in dc conductivity in our nanoparticles is observed at doping levels of up to 20% Nb, which is much higher than the doping level of ~4% in the bulk materials grown by physical methods or solid-state high-temperature synthesis[17−19] with a much more perfect and defect-free crystalline lattice. The strong localization of the reduced states also explains the low dc conductivity in as-prepared particles. Thermal annealing then decreases the lattice defect density, which leads to the improvement of the dc conductivity. However, we emphasize that the electron transport still occurs by hopping and the electron dc mobility is thus still much lower than that found in bulk anatase crystals.

5. CONCLUSION

Time-domain terahertz transmission spectroscopy and microwave impedance spectroscopy were used to investigate dielectric and conduction properties of undoped and Nb-doped TiO_2 mesoporous pellets in a wide frequency range (20 MHz−1 THz). A model accounting for the inhomogeneous nature of the pellets was developed; it was shown that the percolation of the titania significantly increases upon annealing. The terahertz and microwave response of titania nanoparticles is dominated by charge hopping and by the tail of phonon modes. We conclude that the transport of a vast majority of electrons in the doped samples occurs by hopping (= low mobility) between the reduced states and not by the free electron motion in delocalized conduction band states (= high mobility). The dielectric losses in titania nanoparticles are higher than in the bulk. Thermal annealing of doped samples reduces their high-frequency saturated hopping conductivity and their dielectric loss, which point to lattice improvement upon annealing.

AUTHOR INFORMATION

Corresponding Author
*E-mail nemec@fzu.cz.

ACKNOWLEDGMENT

This work was supported by the Czech Science Foundation (202/09/P099), Academy of Sciences of the Czech Republic (A100100902, AVOZ10100520), the Ministry of Education of the Czech Republic (LC-512), the German Research Foundation (DFG, Grant FA 839/1-1), Nanosystems Initiative Munich (NIM), and LMUexcellent funded by the DFG. Y.L. is grateful to the Siemens/DAAD program for a postgraduate scholarship.

REFERENCES

(1) Hegmann, F. A.; Ostroverkhova, O.; Cooke, D. G. In *Photophysics of Molecular Materials*; Wiley−VCH: New York, 2006; pp 367−428.

(2) Fekete, L.; Kužel, P.; Němec, H.; Kadlec, F.; Dejneka, A.; Stuchlík, J.; Fejfar, A. *Phys. Rev. B* **2009**, *79*, No. 115306.
(3) Němec, H.; Kužel, P.; Sundström, V. *Phys. Rev. B* **2009**, *79*, No. 115309.
(4) Němec, H.; Kužel, P.; Sundström, V. *J. Photochem. Photobiol. A* **2010**, *215*, 123.
(5) Hendry, E.; Koeberg, M.; O'Regan, B.; Bonn, M. *Nano Lett.* **2006**, *6*, 755.
(6) Němec, H.; Kužel, P.; Kadlec, F.; Fattakhova-Rohlfing, D.; Szeifert, J.; Bein, T.; Kalousek, V.; Rathouský, J. *Appl. Phys. Lett.* **2010**, *96*, No. 062103.
(7) Furubayashi, Y.; Hitosugi, T.; Yamamoto, Y.; Inaba, K.; Kinoda, G.; Hirose, Y.; Shimada, T.; Hasegawa, T. A. *Appl. Phys. Lett.* **2005**, *86*, No. 252101.
(8) Liu, Y.; Szeifert, J. M.; Feckl, J. M.; Mandlmeier, B.; Rathouský, J.; Hayden, O.; Fattakhova-Rohlfing, D.; Bein, T. *ACS Nano* **2010**, *4*, 5373.
(9) Grüner, G. *Millimeter and submillimeter wave spectroscopy of solids*; Springer-Verlag: Berlin and Heidelberg, Germany, 1998.
(10) Kužel, P.; Němec, H.; Kadlec, F.; Kadlec, C. *Opt. Exp.* **2010**, *18*, 15338.
(11) Duvillaret, L.; Garet, F.; Coutaz, J.-L. *Appl. Opt.* **1999**, *38*, 409.
(12) Gonzalez, R. J.; Zallen, R.; Berger, H. *Phys. Rev. B* **1997**, *55*, 7014.
(13) Elliott, S. R. *Adv. Phys.* **1987**, *36*, 135.
(14) Dyre, J. C. *J. Appl. Phys.* **1988**, *64*, 2456.
(15) Kadlec, C.; Kadlec, F.; Kužel, P.; Blary, K.; Mounaix, P. *Opt. Lett.* **2008**, *33*, 2275.
(16) Petzelt, J.; Kamba, S. *Mater. Chem. Phys.* **2003**, *79*, 175.
(17) Furubayashi, Y.; Yamada, N.; Hirose, Y.; Yamamoto, Y.; Otani, M.; Hitosugi, T.; Shimada, T.; Hasegawa, T. *J. Appl. Phys.* **2007**, *101*, No. 212106.
(18) Haosugi, T.; Ueda, A.; Nakao, S.; Yamada, N.; Furubayashi, Y.; Hirose, Y.; Konuma, S.; Shimada, T.; Hasegawa, T. *Thin Solid Films* **2008**, *516*, 5750.
(19) Zhang, S. X.; Kundaliya, D. C.; Yu, W.; Dhar, S.; Young, S. Y.; Salamanca-Riba, L. G.; Ogale, S. B.; Vispute, R. D.; Venkatesan, T. *J. Appl. Phys.* **2007**, *102*, No. 013701.